Observation of Plasma Toroidal-Momentum Dissipation by Neoclassical Toroidal Viscosity

W. Zhu,[1] S. A. Sabbagh,[1] R. E. Bell,[2] J. M. Bialek,[1] M. G. Bell,[2] B. P. LeBlanc,[2] S. M. Kaye,[2] F. M. Levinton,[3] J. E. Menard,[2] K. C. Shaing,[4] A. C. Sontag,[1] and H. Yuh[3]

[1]*Department of Applied Physics and Applied Mathematics, Columbia University, New York, New York 10027, USA*
[2]*Princeton Plasma Physics Laboratory, Princeton University, Princeton, New Jersey 08543, USA*
[3]*Nova Photonics, Princeton University, Princeton, New Jersey 08543, USA*
[4]*University of Wisconsin, Madison, Wisconsin 53706, USA*

(Received 17 March 2006; published 9 June 2006)

Dissipation of plasma toroidal angular momentum is observed in the National Spherical Torus Experiment due to applied nonaxisymmetric magnetic fields and their plasma-induced increase by resonant field amplification and resistive wall mode destabilization. The measured decrease of the plasma toroidal angular momentum profile is compared to calculations of nonresonant drag torque based on the theory of neoclassical toroidal viscosity. Quantitative agreement between experiment and theory is found when the effect of toroidally trapped particles is included.

DOI: 10.1103/PhysRevLett.96.225002 PACS numbers: 52.35.Py, 52.55.Fa, 52.55.Tn, 52.65.Kj

Maximum fusion power production is reached in high pressure tokamak plasmas by avoiding or stabilizing significant magnetohydrodynamic (MHD) instabilities, such as tearing modes, kink-ballooning modes, and resistive wall modes (RWMs) [1–3]. Plasma rotation can contribute to the stabilization of these modes by shielding static, three-dimensional error fields and by dissipating free energy available to the instabilities [4,5]. However, stabilizing rotation is often dissipated in tokamaks by drag torques, theoretically predicted to occur by several different mechanisms including plasma fluid viscosity [6], interaction of error fields with tearing mode generated currents [7], and interaction of the plasma fluid and magnetic field perturbations [8]. Understanding of the physical mechanisms responsible for plasma momentum dissipation is needed to determine how the favorable plasma rotation can be sustained and maximized, or how the plasma rotation profile might be controlled in future tokamaks.

While there has been success in understanding radially localized damping by tearing instabilities tied to rational magnetic surfaces [9] (resonant damping mechanisms), quantitative understanding of nonresonant momentum dissipation observed in experiments has been elusive. Neoclassical toroidal viscosity [10] (NTV) is a viable theory of plasma momentum dissipation for these observations. NTV is caused by interaction of the plasma with magnetic field components that break the toroidal symmetry of the magnetic confinement field in a tokamak [11,12]. Using a fluid model, NTV drag can be described as the force on the plasma fluid as it flows through the nonaxisymmetric field perturbation. Using a particle model, the drag can be described in a relatively collisional plasma as a toroidal force caused by a radial nonambipolar flux of particles drifting due to the nonaxisymmetric field. In a collisionless plasma, the effect is dominated by trapped particle drifts. Experimental comparison to theory has included semiempirical application to tearing modes in DIII-D [13] and comparison to the plateau regime formulation using cylindrical approximations in JET [14] and NSTX [15]. The JET study found qualitative agreement to the measured global damping, but determined that the theory underestimated the observed damping by a few orders of magnitude. A more recent JET study discussed a rough estimate of the increase in NTV magnitude expected in the collisionless regime [16]. In the present study, NTV theory appropriate for all collisionality regimes is quantitively compared to experimental results from the National Spherical Torus Experiment [17] (NSTX). A significant conclusion of the present work is that theory and experiment agree to order one.

Nonaxisymmetric magnetic field perturbations were generated in NSTX by applying the field externally, by amplifying this field by plasma pressure (resonant field amplification (RFA) due to stable MHD modes [18]), and by allowing RWMs to become unstable. NSTX is especially well suited for this study since the relatively small plasma moment of inertia at the low device aspect ratio, $A \sim 1.3$ results in greater sensitivity of the plasma rotation to changes in torque. The device can generate applied fields with dominant toroidal mode number from 1 to 3, using six nominally rectangular, toroidally conformed, dual-turn coils centered on the device midplane with $R = 1.757$ m (external to the vacuum vessel) and half-height of 0.483 m. Each coil subtends approximately 60 degrees of toroidal angle. Plasma rotation is measured at 51 locations across the outboard major radius at the device midplane by a charge exchange recombination spectroscopy (CHERS) diagnostic using emission from C^{5+} at 5290 Å.

The theoretical formulation of NTV by Shaing, *et al.* is expressed in Hamada coordinates (θ, ζ), which are computed from experimental equilibrium reconstructions [19] including magnetic pitch angle data from a motional Stark effect diagnostic and used in the calculations in this Letter. The magnitude of the three-dimensional magnetic field on each flux surface is decomposed into both poloidal, m, and toroidal, n, components as

$$B = B_0\left(1 + \sum_{n,m\neq 0} B_{nm}(\theta,\zeta)\right) = B_0\left(1 + \sum_{n,m\neq 0} [B_{nmc}\cos(m\theta - n\zeta) + B_{nms}\sin(m\theta - n\zeta)]\right). \quad (1)$$

The notation $n, m \neq 0$ means that n and m are not simultaneously zero. The flux surface-averaged force on the plasma due to neoclassical toroidal viscosity in the plateau and collisional transport regimes [10,20] is defined as

$$\langle \hat{e}_t \bullet \vec{\nabla} \bullet \vec{\vec{\Pi}} \rangle_p = 2\sqrt{\pi} p_i (V \bullet \vec{\nabla}\zeta) \sum_{n,m\neq 0} \left(\left\langle \frac{\vec{B}_t \bullet \vec{\nabla} B}{B_t B} \frac{\partial B_{nm}}{\partial \zeta} \right\rangle \frac{\mu_{ps1}}{\frac{2\sqrt{\pi}}{3}\nu_i + \mu_{ps1}\frac{V_{Ti}}{R_0 q}|m - nq|} \right), \quad (2)$$

where p_i is the ion plasma pressure, V is the plasma fluid velocity, V_{Ti} is the ion thermal speed, ν_i is the ion collision frequency as defined in Ref. [21], q is the safety factor, R_0 is the flux surface major radius at the midplane, $\mathbf{B}$ and $\mathbf{B_t}$ are the total and the toroidal magnetic field, respectively, $B = |\mathbf{B}|$, $B_t = |\mathbf{B_t}|$, $e_t = \mathbf{B_t}/|\mathbf{B_t}|$, $\mathbf{\Pi}$ is the ion viscous stress tensor, $\mu_{ps1} = 1.365$, and $\langle \ldots \rangle$ denotes an average over the flux surface. Equation (2) reduces to

$$\langle \hat{e}_t \bullet \vec{\nabla} \bullet \vec{\vec{\Pi}} \rangle_p = \frac{\sqrt{\pi} p_i}{V_{Ti}} \Omega_\phi q \left(R_0 R \left\langle \frac{1}{R^2} \right\rangle B_0 B_t \left\langle \frac{1}{B B_t} \right\rangle \right) \sum_{n,m\neq 0} \left(n^2 (B_{nmc}^2 + B_{nms}^2) \frac{\mu_{ps1}}{\frac{2\sqrt{\pi}}{3}\frac{\nu_i}{(\frac{V_{Ti}}{R_0 q})} + \mu_{ps1}|m - nq|} \right), \quad (3)$$

which is used for the computation. Here, Ω_ϕ is the plasma toroidal rotation frequency and R is the major radial coordinate. The equivalent NTV formulation for the collisionless regime can be derived from Ref. [21] as

$$\langle \hat{e}_t \bullet \vec{\nabla} \bullet \vec{\vec{\Pi}} \rangle_{(1/\nu)} = B_t R \left\langle \frac{1}{B_t} \right\rangle \left\langle \frac{1}{R^2} \right\rangle \frac{\lambda_{1i} p_i}{\pi^{3/2} \nu_i} \Omega_\phi I_\lambda, \quad (4)$$

where

$$I_\lambda = \frac{\varepsilon^{3/2}}{\sqrt{2}} \left[\int_0^1 d\kappa^2 [E(\kappa) - (1 - \kappa^2)K(\kappa)]^{-1} \sum_n n^2 \left\{ \begin{array}{l} [\oint d\theta (\kappa^2 - \sin^2(\theta/2))^{1/2} A_n]^2 + \\ [\oint d\theta (\kappa^2 - \sin^2(\theta/2))^{1/2} B_n]^2 \end{array} \right\} \right], \quad (5)$$

$\varepsilon \equiv r/R_0$, r is the minor radial coordinate, and $\lambda_{1i} \equiv 13.708$. The independent integration variable κ is a normalized pitch angle parameter defined in Ref. [21]. The functions $K(\kappa)$ and $E(\kappa)$ are the complete elliptic integrals of the first and second kind, respectively, and the contour integration is taken over the bounce orbit $\oint d\theta = 2\int_0^{2\arcsin(\kappa)} d\theta$. The Fourier coefficients A_n, B_n for the magnetic field B as defined in Equation (6) of Ref. [21] are generalized by B_{nmc} and B_{nms}. Equation (5) reduces to

$$I_\lambda = \frac{\varepsilon^{3/2}}{\sqrt{2}} \sum_{n,m\neq 0} n^2 (B_{nmc}^2 + B_{nms}^2) W_{nm}, \quad (6)$$

which is used for the computation of Eq. (4). Here,

$$W_{nm} = \int_0^1 d\kappa^2 \frac{|(F_{nmc}(\kappa))^2 + (F_{nms}(\kappa))^2|}{[E(\kappa) - (1 - \kappa^2)K(\kappa)]}, \quad (7)$$

and

$$F_{nmc}(\kappa) = \oint d\theta (\kappa^2 - \sin^2(\theta/2))^{1/2} \cos((m - nq)\theta), \quad (8)$$

$$F_{nms}(\kappa) = \oint d\theta (\kappa^2 - \sin^2(\theta/2))^{1/2} \sin((m - nq)\theta). \quad (9)$$

Quantitative agreement between the theory and experiment relies on the inclusion of a broad spectrum when computing B_{nmc} and B_{nms}, rather than simply one resonant component and/or sidebands. The applied nonaxisymmetric field is determined by a Biot-Savart calculation using a detailed 3D numerical model of the nonaxisymmetric coils as built, given the measured coil currents. The variation of $|\mathbf{B}|$ as a function of toroidal angle, ϕ, and R is shown in Fig. 1(a) for coil currents primarily generating an $n = 1$ radial field. This field is then decomposed to determine B_{nmc} and B_{nms} by Eq. (1) with $(0 < n < 15)$, and $(-15 < m < 15)$. The decomposition of $|\mathbf{B}|$ is shown at the plasma midplane ($\theta = 0$) in Fig. 1(b) by the quantity B_{ns}, where $B_{ns,c} \equiv \sum_m B_{nms,c}$. The relevant NTV quantity $n^2(B_{nc}^2 + B_{ns}^2)$ plotted in Fig. 1(c) shows that the viscosity is more strongly influenced by the $n = 5$ component, with $n = 11$ also contributing. For a current configuration selected to primarily generate an $n = 3$ radial field at the midplane, the dominant terms for this quantity are $n = 3$ and $n = 9$. Experimentally, the effect of the applied field on the plasma lags the time of application as the field penetrates the hot, rapidly rotating core plasma which has reached rotation frequencies normalized to the Alfvén frequency of 0.48 [22]. The nonaxisymmetric field in vacuum is therefore shielded in the plasma core by the rotating plasma using a factor $1/(1 + \Omega_\phi^2 \tau^2)^{0.5}$. The field is taken to penetrate completely at radii between 50%–100% of the poloidal flux, and the profile of τ inside this radius is matched to the core rotation damping profile shape using several discharges and applied to all equilibria tested. The change in the measured plasma angular momentum profile is compared to the theoretical NTV torque by evaluating the angular equation of motion $d(I\Omega_\phi)/dt = \Sigma T_j$, where the torques T_j are due to: (i) NTV, T_{NTV}, (ii) momentum input from high-power coinjected neutral beams, T_{NBI}, (iii) electromagnetic forces on rotating magnetic islands (resistive MHD modes), T_{JxB}, and (iv) fluid viscous forces between adjacent flux surfaces, $T_{\mu\perp}$. MHD theory shows that Ω_ϕ

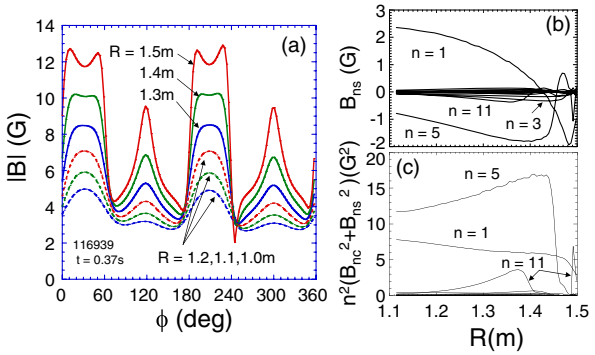

FIG. 1 (color online). (a) $|\mathbf{B}|$ vs toroidal angle and major radius for nonaxisymmetric field coil currents yielding a radial magnetic field with dominant $n = 1$ component, (b) major radial profile of toroidal mode number spectrum (sine component) of this field, and (c) flux surface-averaged field component summation $n^2(B_{nc}{}^2 + B_{ns}{}^2)$ relevant to the NTV calculation.

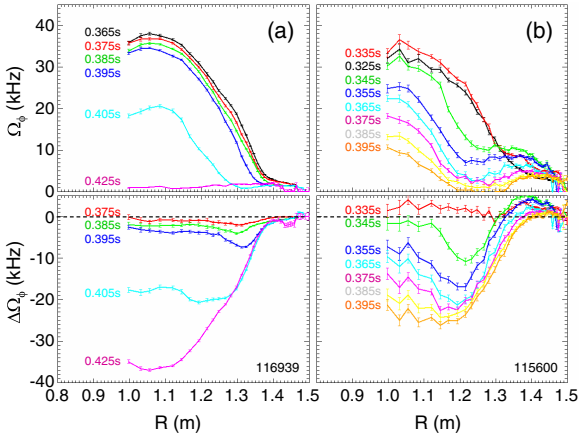

FIG. 2 (color online). Toroidal plasma rotation profile vs major radius, and the difference between initial profile and subsequent profiles for rotation damping (a) during application of nonaxisymmetric field, and (b) during excitation of rotating tearing instability.

is constant on a flux surface, each of which is considered a thin, inertial toroidal shell with moment of inertia, I. The plasma mass density, ρ, is measured at the plasma midplane. The total integrated torque over the flux surface due to NTV, $T_{\mathrm{NTV}} = T_{\mathrm{NTV}-p} + T_{\mathrm{NTV}-(1/\nu)}$, where $T_{\mathrm{NTV}-p,(1/\nu)} = R_0 V_a \langle \hat{e}_t \bullet \vec{\nabla} \bullet \vec{\Pi} \rangle_{p,(1/\nu)}$, and V_a is the volume of the inertial shell. Experimentally, T_{NTV} is isolated by allowing the plasma rotation profile to reach a quasi-steady state, so that $T_{\mathrm{NBI}}|_0 = -(T_{JxB} + T_{\mu\perp} + T_{\mathrm{NTV}})|_0$. After this time, the nonaxisymmetric field is applied. The differences between $T_{JxB}|_0$, $T_{\mu\perp}|_0$, $T_{\mathrm{NBI}}|_0$, and their values at later times of interest are significantly smaller than $T_{\mathrm{NTV}}(t)$. The experiment is conducted during periods when significant tearing instabilities are absent, so T_{JxB} is itself small. The plasma rotation profile evolution due to tearing modes is distinct from NTV-induced rotation damping so their lack of influence on rotation drag can be verified [15]. This is illustrated in Fig. 2, where the rotation damping observed in the present experiments [Fig. 2(a)] is contrasted with rotation damping due to T_{JxB} [Fig. 2(b)]. The damping due to NTV is relatively rapid, global, and the rotation profile decays in a self-similar fashion. In contrast, the damping due to T_{JxB} is initially localized near the island, and diffusive from this radius, leading to a local flattening of Ω_ϕ and a distinctive momentum diffusion across the rational surface from smaller to larger R as expected by theory [7,9]. Also, $T_{\mu\perp} \ll T_{\mathrm{NTV}}$ can be shown by first measuring the magnitude of $\mu_\perp$ in similar plasmas that exhibit radially localized tearing modes. Applying the measured value of $\mu_\perp$ using the plasma illustrated in Fig. 2(b) at $t = 0.395$ s to the NTV momentum dissipation experiment in Fig. 2(a), we find that $T_{\mu\perp} < 0.15\ T_{\mathrm{NTV}}$ at the peak value of T_{NTV} between $t = 0.355$–0.375 s. Finally, $(T_{\mathrm{NBI}} - T_{\mathrm{NBI}}|_0) \ll T_{\mathrm{NTV}}$ is independently verified using the TRANSP code. The plasma shown in Fig. 3 has $(T_{\mathrm{NBI}} - T_{\mathrm{NBI}}|_0)/T_{\mathrm{NTV}} = 0.02$ at the peak value of T_{NTV}. With these assumptions, the equation of motion during times of interest becomes $d(I\Omega_\phi)/dt = T_{\mathrm{NTV}}$, which is evaluated on reconstructed equilibrium flux surfaces.

The plasma toroidal-momentum dissipation is first evaluated at values of β_N below the $n = 1$ ideal no-wall beta limit, $\beta_N^{\text{no-wall}}$, the time evolution of which is evaluated by the DCON [23] ideal MHD stability code. When $\beta_N < \beta_N^{\text{no-wall}}$, beta effects such as RFA are insignificant, so the nonaxisymmetric field that penetrates the plasma can be modeled simply as the vacuum field modified by shielding caused by plasma rotation. Comparison of the measured dissipation of plasma angular momentum caused by the externally applied nonaxisymmetric fields to the theoretical NTV torque profile is shown in Fig. 3 for an $n = 3$ applied field configuration. The measured value of $d(I\Omega_\phi)/dt$ includes error bars that take into account the uncertainty in Ω_ϕ and ρ.

As β_N approaches and exceeds $\beta_N^{\text{no-wall}}$, RFA is measured as the applied nonaxisymmetric field is amplified by the weakly stabilized RWM and needs to be included in the calculation of T_{NTV}. The RFA magnitude is defined as the

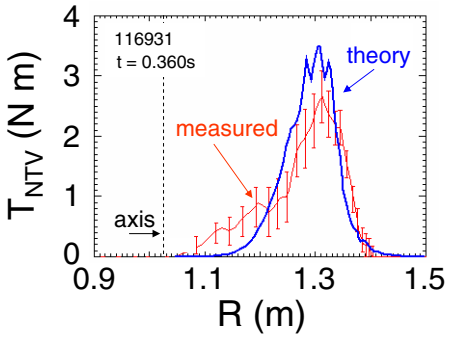

FIG. 3 (color online). Comparison of measured $d(I\Omega_\phi)/dt$ profile to theoretical integrated NTV torque for an $n = 3$ applied field configuration.

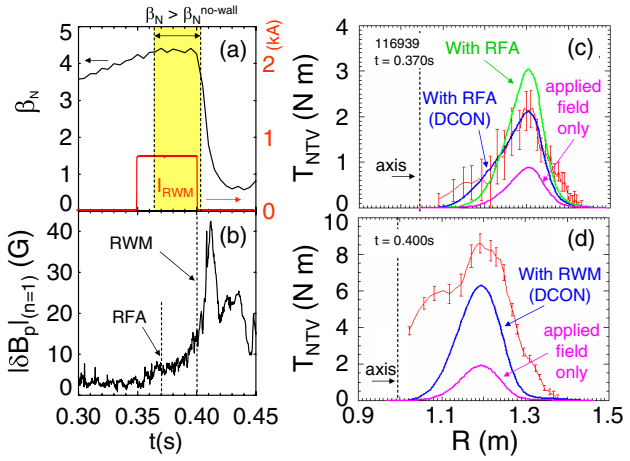

FIG. 4 (color online). NTV during amplification of $n = 1$ nonaxisymmetric field configuration: (a) evolution of β_N, computed period when $\beta_N > \beta_N^{\text{no-wall}}$, and maximum current in nonaxisymmetric field coils; (b) $n = 1$ plasma response measured by poloidal field sensors; (c) comparison of measured $d(I\Omega_\phi)/dt$ profile to theoretical integrated NTV torque during RFA; and (d) similar comparison during RWM evolution.

ratio of the plasma-induced field amplitude (measured field minus applied vacuum field) to the applied vacuum field amplitude from magnetic sensors interior to the vacuum vessel. As the rotation decreases below a critical profile, the field grows more strongly and rapidly as the RWM becomes unstable. The evolution of β_N, its relation to the DCON computed $\beta_N^{\text{no-wall}}$, the timing of the applied field, and the plasma response to this field are shown in Figs. 4(a) and 4(b) for an $n = 1$ nonaxisymmetric field configuration. The field amplification used in T_{NTV} is computed in two ways for comparison: (i) during early periods of RFA, the field is increased by multiplying the $n = 1$–3 components of the applied field by the measured RFA magnitude and (ii) during stronger RFA, or if the RWM becomes unstable, the field of the mode is modeled using the theoretical eigenfunction computed using DCON. The poloidal mode decomposition of this eigenfunction is computed for each $n = 1$–3, multiplied by the measured RFA magnitude, then added to B_{nmc} and B_{nms} computed from the applied field. The results using each technique are shown in Fig. 4(c) for the earlier time in the discharge when the RFA is relatively weak. The second technique gives a slightly better result, and is used for the later time [see Fig. 4(d)] when the RWM becomes unstable. In both frames, T_{NTV} is also shown using the nonamplified applied field for comparison. The RWM case [Fig. 4(d)] clearly shows measured Ω_ϕ damping at the magnetic axis that does not match the theory due to the $\varepsilon^{1.5}$ dependence. This mismatch is likely due to momentum diffusion caused by $T_{\mu\perp}$ that becomes more prominent away from the peak of T_{NTV} and late in time during the Ω_ϕ damping evolution. The difference in peak values between theory and experiment can be attributed in part to uncertainty in evaluating the RFA magnitude.

Similar analyses were conducted for 30 different equilibria with varying levels of nonaxisymmetric field amplification. The ratio $(T_{\text{NTV}})/(d(I\Omega_\phi)/dt)$ using the peak values along the radial profile for this ensemble of equilibria has a mean value of 1.59 with standard deviation of 0.87. This is significantly closer agreement than found in previous studies. Also, the radial peak of the measured and computed profiles vary in alignment by 2.28 cm $\pm$ 1.71 cm. This small misalignment might be due in part to alteration of the reconstructed equilibrium by the nonaxisymmetric field and the 10 ms averaging time of the CHERS diagnostic.

Quantitative agreement between theory and experiment in this study shows NTV theory as viable physics to be included in studies of torque balance in tokamak plasmas. The agreement also suggests it as a possible energy dissipation mechanism to be included in stability analysis of modes such as the RWM [24]. Its inclusion may help solve present outstanding issues found in both areas of research, giving greater confidence to predictive models of plasma behavior. Further research is planned to investigate the ion collisionality and aspect ratio dependence of T_{NTV}.

The authors thank Dr. J. D. Callen and Dr. C. C. Hegna for informative discussions. This research was supported by U.S. Department of Energy Contracts No. DE-FG02-99ER54524 and No. DE-AC02-76CH03073.

[1] A. Bondeson and D. J. Ward, Phys. Rev. Lett. **72**, 2709 (1994).
[2] A. M. Garofalo *et al.*, Phys. Rev. Lett. **82**, 3811 (1999).
[3] S. A. Sabbagh *et al.*, Phys. Plasmas **9**, 2085 (2002).
[4] R. Betti and J. P. Friedberg, Phys. Rev. Lett. **74**, 2949 (1995).
[5] A. M. Garofalo *et al.*, Nucl. Fusion **40**, 1491 (2000).
[6] F. L. Hinton and R. D. Hazeltine, Rev. Mod. Phys. **48**, 239 (1976).
[7] R. Fitzpatrick, Nucl. Fusion **33**, 1049 (1993).
[8] K. C. Shaing *et al.*, Phys. Rev. Lett. **80**, 5353 (1998).
[9] M. Yokoyama *et al.*, Nucl. Fusion **36**, 1307 (1996).
[10] K. C. Shaing *et al.*, Phys. Fluids **29**, 521 (1986).
[11] A. I. Smolyakov *et al.*, Phys. Plasmas **2**, 1581 (1995).
[12] K. C. Shaing, Phys. Rev. Lett. **87**, 245003 (2001).
[13] R. J. La Haye *et al.*, Phys. Plasmas **9**, 2051 (2002).
[14] E. Lazzaro *et al.*, Phys. Plasmas **9**, 3906 (2002).
[15] S. A. Sabbagh *et al.*, Nucl. Fusion **44**, 560 (2004).
[16] E. Lazzaro and P. Zanca, Phys. Plasmas **10**, 2399 (2003).
[17] S. M. Kaye *et al.*, Nucl. Fusion **45**, S168 (2005).
[18] A. H. Boozer, Phys. Rev. Lett. **86**, 5059 (2001).
[19] S. A. Sabbagh *et al.*, Nucl. Fusion **41**, 1601 (2001).
[20] K. C. Shaing, Phys. Fluids B **5**, 3841 (1993).
[21] K. C. Shaing, Phys. Plasmas **10**, 1443 (2003).
[22] S. A. Sabbagh *et al.*, Nucl. Fusion **46**, 635 (2006).
[23] A. H. Glasser and M. C. Chance, Bull. Am. Phys. Soc. **42**, 1848 (1997); W. Newcomb, Ann. Phys. (N.Y.) **10**, 232 (1960).
[24] M. S. Chu *et al.*, Phys. Plasmas **2**, 2236 (1995).